

How can Diffusion Models Evolve into Continual Generators?

Jingren Liu^{1,2}, Zhong Ji^{1*}, Xiangyu Chen^{2*}

¹ Tianjin University, Tianjin, China.

² Institute of Artificial Intelligence, ChinaTelecom, Shanghai, China.
jr10219@tju.edu.cn, jizhong@tju.edu.cn, chxy95@gmail.com

Abstract

While diffusion models have achieved remarkable success in static data generation, their deployment in streaming or continual learning (CL) scenarios faces a major challenge: catastrophic forgetting (CF), where newly acquired generative capabilities overwrite previously learned ones. To systematically address this, we introduce a formal Continual Diffusion Generation (CDG) paradigm that characterizes and redefines CL in the context of generative diffusion models. Prior efforts often adapt heuristic strategies from continual classification tasks but lack alignment with the underlying diffusion process. In this work, we develop the first theoretical framework for CDG by analyzing cross-task dynamics in diffusion-based generative modeling. Our analysis reveals that the retention and stability of generative knowledge across tasks are governed by three key consistency criteria: inter-task knowledge consistency (IKC), unconditional knowledge consistency (UKC), and label knowledge consistency (LKC). Building on these insights, we propose Continual Consistency Diffusion (CCD), a principled framework that integrates these consistency objectives into training via hierarchical loss terms \mathcal{L}_{IKC} , \mathcal{L}_{UKC} , and \mathcal{L}_{LKC} . This promotes effective knowledge retention while enabling the assimilation of new generative capabilities. Extensive experiments on four benchmark datasets demonstrate that CCD achieves state-of-the-art performance under continual settings, with substantial gains in Mean Fidelity (MF) and Incremental Mean Fidelity (IMF), particularly in tasks with rich cross-task knowledge overlap.

1 Introduction

The remarkable success of diffusion models in synthesizing high-fidelity images has significantly accelerated the arrival of generative artificial intelligence (AGI). However, the static nature of their training paradigm hinders further advancement in dynamic real-world scenarios, such as personalized content creation platforms or real-time virtual environment generation for interactive applications. When faced with the arrival of new data, existing approaches generally involve retraining models on both historical and current data to prevent significant performance degradation or generative collapse² on previously learned tasks. However, this is computationally expensive and results in considerable waste of both computational resources and energy, exacerbating the practical challenges of deploying diffusion models in continual learning (CL) contexts. As a result, the need for an effective and stable Continual Diffusion Generation (CDG) framework has become increasingly urgent.

While recent efforts have proposed a variety of promising strategies to mitigate catastrophic forgetting (CF) phenomenon in generative models, most remain insufficiently aligned with the core dynamics

*Corresponding authors.

²During the training of streaming tasks, we observe that diffusion models occasionally experience sudden catastrophic failures on certain tasks, leading to a significant degradation in performance.

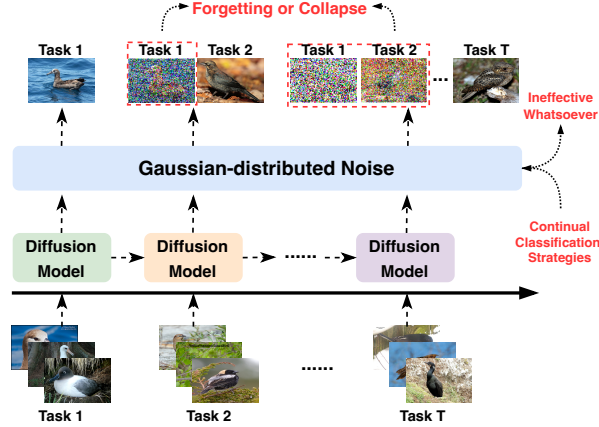


Figure 1: An overview of Continual Diffusion Generation and its associated challenges. Current continual classification methods are largely ineffective, and often counterproductive, in preventing performance degradation and generative collapse in streaming tasks with diffusion models.

of diffusion-based architectures. In particular, many approaches adopt heuristics from continual classification tasks [33, 25, 34, 46, 20], or borrow stability-plasticity trade-off mechanisms originally developed for Generative Adversarial Networks (GANs) [1, 41, 42, 6, 48]. These techniques often conflict with the stochastic differential equations (SDEs) that govern the generative process in diffusion models, leading to noticeable degradation in output quality. Empirical results confirm these limitations, showing consistent declines in generative fidelity across sequential tasks reflected in metrics such as Fréchet Inception Distance (FID) (see Fig.1 and Tab.1). Therefore, to improve this situation, we begin by analyzing the mechanisms inherent in diffusion models and explore how they should be optimized in the context of streaming tasks to preserve shared knowledge across tasks as much as possible, thereby mitigating CF phenomenon in CDG.

To achieve this goal, we begin by formalizing diffusion trajectories, complex sequences of denoising operations that progressively transform noise into structured outputs, and examining how they interact through shared knowledge under streaming task scenarios. Grounded in Bayesian theory and multi-task learning principles [44], we derive a theoretical upper bound that quantifies the retention of generative knowledge across tasks in CDG, as formally defined in Theorem 1. Attaining this upper bound requires satisfying three critical consistency constraints: inter-task alignment of model-internalized knowledge, consistency in the mean embeddings of unconditional samples across tasks, and semantic consistency within the prior (i.e., label) space of original samples³ across tasks.

To operationalize the theoretical insights, we introduce the Continual Consistency Diffusion (CCD) framework, which translates the derived guarantees into a tractable, consistency-driven optimization strategy. CCD enforces cross-task stability through a hierarchical integration of consistency objectives. Specifically, *Inter-task Knowledge Consistency* regularizes model-internal knowledge representations across tasks, serving as the foundation for long-term retention. *Unconditional Knowledge Consistency* preserves intrinsic generative behavior in the absence of explicit human priors, ensuring temporal coherence in the denoising process. Complementarily, *Label Knowledge Consistency* promotes alignment in the label space by enforcing semantic correspondence between original samples across tasks. Collectively, these mechanisms move beyond standard regularization or classification heuristics. By directly constraining the geometric structure of the diffusion process, CCD enables robust and theoretically grounded continual generation.

In doing so, our work bridges the critical gap between traditional static diffusion models and the dynamic nature of real-world data streams. We present three main contributions. First, to the best of our knowledge, we are the first to rigorously formulate CDG from a diffusion perspective, rather than repurposing continual classification methods as done in previous studies. Second, we establish the first theoretical framework for CDG rooted in stochastic calculus, introducing novel stability bounds for SDE trajectories under sequential task adaptation (Theorem 1). Third, guided by these insights, we propose the CCD framework, which enforces intrinsic knowledge consistency through

³Notably, the label space in our setting serves as a proxy for human prior knowledge, and the constraint is not imposed to improve classification performance, but rather to preserve shared semantic structure across tasks.

three synergistic components. Experiments on four benchmarks demonstrate its superiority, yielding significant gains while effectively mitigating CF phenomenon and generative collapse.

2 Related Works

Diffusion Models. Diffusion-based generative architectures have redefined state-of-the-art performance in structured data synthesis, primarily due to their ability to invert stochastic denoising trajectories. At a foundational level, these models learn to reverse-engineer discrete Markov chains (DDPMs) [9] or continuous-time stochastic differential equations (SDEs) [32]. Recent advancements in noise scheduling [22, 19] and adaptive sampling techniques [19, 49] have further enhanced output fidelity. Such developments underscore diffusion models’ theoretical strength as universal data approximators [31], regardless of their discrete or continuous formulation. However, their success heavily relies on closed-world assumptions, where training data remains static and entirely observable. Consequently, a critical challenge persists in adapting diffusion models to dynamic, streaming data environments, paralleling incremental human cognition.

Continual Learning. Continual Learning (CL) aims to enable models to progressively acquire new knowledge while retaining previously learned information, addressing the challenge of CF [12, 16, 24]. Traditional CL methodologies include replay-based techniques, which store subsets of historical data to maintain stable performance [26], and regularization methods like EWC [12] and LwF [16], which impose constraints on parameters to reduce interference between tasks. Additionally, gradient-based strategies such as GEM [18] orthogonalize gradients to minimize task conflicts. Recent advancements have increasingly emphasized memory efficiency [26] and robustness against domain shifts [24]. In parallel, the advent of pre-training has driven progress in parameter-efficient fine-tuning techniques. Methods such as L2P [40] and DualPrompt [39] utilize task-specific prompts to effectively balance adaptability and knowledge retention. Techniques like S-Prompt [38] and CODA-Prompt [28] enhance performance by explicitly capturing domain relationships, while dynamic methods like DAP [11] and hierarchical approaches like HiDe-Prompt [37] support adaptation across diverse domains. Innovations such as EASE [50] and NTK-CL [17] introduce expandable adapters and hybrid architectures to achieve efficient parameter tuning. Despite these advancements, the existing CL research remains focused on basic classification tasks, limiting applicability to complex real-world scenarios. To bridge this gap, we investigate extending CL methods to practical and challenging applications, particularly in the context of continual diffusion generation.

Continual Diffusion Generation. CDG represents a significant blind spot in the current landscape of CL research, with only a scant body of work dedicated to this area. Among these studies, most have primarily explored methods based on GAN architectures [1, 41, 42, 6, 48]. Additionally, many approaches attempt to adapt techniques originally developed for continual classification problems [33, 25, 34, 46, 20], applying relevant fine-tuning strategies. However, given that generation and classification are fundamentally distinct tasks, such direct transfer is largely impractical. Our experimental findings further highlight that many methods effective in continual classification scenarios fail entirely in generation settings, sometimes even yielding adverse effects. This is primarily due to the substantial knowledge disparity across tasks, which causes the diffusion generator to collapse, a phenomenon we refer to as generative collapse. In this paper, we address this gap by developing a theoretical framework to model the task transition process of diffusion models.

Continual Diffusion Generation. CDG remains a significantly underexplored area within the broader field of CL, with only limited research dedicated specifically to this domain. Among the existing works, the majority have focused on GAN-based approaches [1, 41, 42, 6, 48], while others have attempted to adapt techniques originally designed for continual classification tasks [33, 25, 34, 46, 20] by applying fine-tuning strategies to generative settings. However, this cross-domain transfer is fraught with challenges. Generation and classification differ fundamentally in objective and structure, making many classification-based methods ill-suited for generative scenarios. Our empirical studies reinforce this observation, revealing that methods successful in continual classification often fail, or even harm performance, when directly applied to generative tasks. A central issue is the substantial knowledge shift across generative tasks, which destabilizes the learning dynamics of diffusion models and leads to what we term as generative collapse, a breakdown in the model’s ability to synthesize meaningful outputs. Recent advances have hinted at alternative pathways. For example, [43] shows that diffusion models could maintain high generative quality when trained on temporally correlated video streams, even with minimal continual mechanisms such as small replay

buffers. This finding suggests that some degree of continuity in input distribution, such as temporal redundancy in video data, can naturally reinforce memory and help mitigate forgetting. Nonetheless, such strategies offer only coarse-grained control and lack the precision necessary to manage how generative knowledge is retained or adapted across tasks. This raises a key research question: how can we design principled mechanisms that provide fine-grained control over knowledge consolidation during task transitions in diffusion-based generative systems? In this paper, we tackle this challenge by introducing a theoretical framework that explicitly models task transitions in diffusion models. Our framework not only advances the theoretical understanding of CDG but also paves the way for developing more robust, adaptive, and scalable continual generative systems.

3 Continual Consistency Diffusion

In CDG, we consider a sequence of non-stationary tasks $\{\mathcal{T}_k\}_{k=1}^K$, where each task \mathcal{T}_k is associated with a distinct data distribution $p^k(x_0)$ and a corresponding conditional label distribution $p^k(y|x_0)$. The forward diffusion process for each task is governed by an SDE: $dx_t^k = f_k(x_t^k, t)dt + g_k(t)dw_t$, where $x_t^k \in \mathbb{R}^d$ represents the diffused samples at time t under task \mathcal{T}_k . To build on the derivations in Appendix B and enhance the preservation of shared knowledge across tasks, we employ a direct rehearsal buffer $\mathcal{B}_k^{\text{real}} = \{\hat{x}_0, \hat{y} \sim p^j(x_0, y)\}_{j=1}^{k-1}$,⁴ which stores a limited set of real samples within a fixed storage budget C . This memory mechanism, both in its theoretical formulation and practical implementation, forms the core foundation for the retention of shared knowledge across tasks.

3.1 Theoretical Foundation

A central challenge in CDG is formalizing the interaction of task-specific generative processes through shared SDE dynamics. Existing empirical approaches [30, 48, 46] mainly adapt solutions from continual classification methods, but lack rigorous theoretical guarantees, often leading to CF or rigid fixation. Our analysis begins by establishing fundamental bounds on cross-task knowledge retention, which are essential for systematic CDG. Through rigorous derivation, we obtain Theorem 1.

Theorem 1 (Cross-Task Diffusion Evolution Bound).⁵ *Let \mathcal{T}_i and \mathcal{T}_j represent two tasks in CDG, each characterized by distinct data distributions $p(x_0)$ and $q(x_0)$, along with their respective conditional label distributions $p(y)$ and $q(y)$. The forward processes for these tasks evolve over time as $\{p(x_t)\}_{t=0}^T$ and $\{q(x_t)\}_{t=0}^T$. Assume that for all x_0, y, t , the conditional probability distributions of the two tasks satisfy $p_t(x_t|x_0, y) = q_t(x_t|x_0, y)$. Here, $p_t(x_t|x_0, y)$ refers to the conditional distribution $p(x_t|x_0, y, t)$, and similarly, $q_t(x_t|x_0, y)$ denotes $q(x_t|x_0, y, t)$. Furthermore, let ϵ_θ^p and ϵ_θ^q represent the time-dependent score approximators, or noise estimators, for tasks \mathcal{T}_i and \mathcal{T}_j . Under mild assumptions, we expect that the gradients of the mean functions $\mu(x_t, t)$ and $\nu(x_t, t)$ align, such that $\nabla_{x_t}\mu(x_t, t) \approx \nabla_{x_t}\nu(x_t, t)$, as noted in [44]. Additionally, it is assumed that the variance σ_t^2 at any given time t remains consistent across both tasks. Lastly, we assume that the evolving state x_t does not influence the label y , meaning the label is independent of the diffusion process at any given time step. These conditions enable the potential retention and transfer of knowledge between tasks, leading to the derivation of an optimization upper bound for their interaction.*

There exist constants $\{\kappa, \lambda, \eta\} \subset \mathbb{R}_{>0}$ such that the inter-task discrepancy is uniformly bounded:

$$\mathcal{L}_{UB} = \kappa \mathcal{L}_{IKC} + \lambda \mathcal{L}_{UKC} + \eta \mathcal{L}_{LKC}, \quad (1)$$

where

$$\mathcal{L}_{IKC} = \epsilon_\theta^q - \epsilon_\theta^p, \quad (2)$$

$$\mathcal{L}_{UKC} = \frac{\bar{\alpha}_t^2}{\beta_t^2} [\mu_\theta(x_t, t) - \nu_\theta(x_t, t)], \quad (3)$$

$$\mathcal{L}_{LKC} = \frac{\bar{\alpha}_t}{\beta_t} \mathbb{E}_{p_t(x_0|x_t)} [D_{\text{KL}}(p_t(y|x_0) \parallel q_t(y|x_0))]. \quad (4)$$

In particular, \mathcal{L}_{UB} encapsulates three components: the inter-task knowledge consistency (\mathcal{L}_{IKC}), the unconditional knowledge consistency (\mathcal{L}_{UKC}), and the label knowledge consistency (\mathcal{L}_{LKC}).

⁴We avoid generative replay as it requires generating past samples for each training batch, significantly extending optimization time by two to three times, making it impractical despite its performance benefits.

⁵For a rigorous proof, please refer to Appendix A and Appendix B.

Minimizing \mathcal{L}_{UB} aligns the reverse-time diffusion gradients between tasks \mathcal{T}_i and \mathcal{T}_j , thereby allowing the two tasks to retain as much shared knowledge as possible during the SDE optimization process.

Theorems 1 demonstrates that CF in CDG can be mitigated by enforcing consistency in the model’s internalization of knowledge, the mean of unconditional sample embeddings, and semantic information across original samples. To operationalize these principles, we develop a hierarchical optimization strategy that decomposes the theoretical bounds into tractable loss terms while preserving their information-theoretic foundations. First, we introduce the basic diffusion training loss and \mathcal{L}_{IKC} .

3.2 Basic Diffusion Model Training

To ensure the optimality of the score estimators ϵ_θ^p and ϵ_θ^q within \mathcal{L}_{IKC} for effective subsequent retention and transfer, we define the fundamental training objective for each task \mathcal{T}_k . Following the standard DDPM framework [9, 32], the base objective for conditional generation minimizes the weighted L_2 error between predicted and actual noise:

$$\mathcal{L}_{cond}^k = \mathbb{E}_{t \sim \mathcal{U}(0,T), \epsilon \sim \mathcal{N}(0,I)} [\|\epsilon_\theta(\bar{\alpha}_t x_0 + \bar{\beta}_t \epsilon, t, y) - \epsilon\|_2^2], \quad (5)$$

where $\bar{\alpha}_t$ and $\bar{\beta}_t$ follow the DDPM variance schedule [9], and ϵ represents standard Gaussian noise.

Building on this, to enhance the shared knowledge between different tasks, we incorporate the data from the buffer into the training process. However, instead of random sampling, we concatenate the pairs $\langle x_0, \hat{x}_0 \rangle$, which also facilitates the implementation of Equations 2 to 4. Therefore, in the CDG, the fundamental composite training objective for diffusion models can be expressed as:

$$\mathcal{L}_{base}^k = \mathcal{L}_{cond}^k + \mathbb{E}_{(\hat{x}_0, \hat{y}) \sim \mathcal{B}_k, t, \epsilon} [\|\epsilon_\theta(\bar{\alpha}_t \hat{x}_0 + \bar{\beta}_t \epsilon, t, \hat{y}) - \epsilon\|_2^2]. \quad (6)$$

This formulation theoretically ensures that the diffusion model maintains effective performance across evolving task distributions, thereby providing a stable optimization trajectory and establishing a reliable lower bound for \mathcal{L}_{IKC} .

3.3 Inter-task Knowledge Consistency

In CDG, the inter-task knowledge consistency term, formulated as $\mathcal{L}_{IKC} = \epsilon_\theta^q - \epsilon_\theta^p$, serves as a critical metric to quantify the divergence between score approximators across tasks. Unlike continual classification, where L2-regularization techniques [29] may offer moderate performance improvements, their direct application in generative settings can induce catastrophic degradation, severely impairing the model’s generative capability, as evidenced in Tab. 1. To circumvent this limitation, we introduce a new knowledge retention strategy, drawing inspiration from [8], where the previously learned score estimator ϵ_θ^p acts as a teacher to guide the adaptation of ϵ_θ^q . In contrast to conventional knowledge distillation techniques [8], which primarily manipulate class probability distributions, our approach capitalizes on the stochastic gradients governed by the reverse-time SDE. This sophisticated formulation not only facilitates an exceptionally seamless and cohesive knowledge retention but also profoundly mitigates the propensity for CF, thereby preserving generative fidelity across successive tasks.

Let \mathcal{M}_{k-1} denote the frozen diffusion model for task \mathcal{T}_{k-1} , parameterized by θ_{k-1} . For a new task \mathcal{T}_k , we seek to adapt θ_k while preserving the score-matching capability on prior tasks. To achieve this, we minimize the Bregman divergence [27] between the score distributions of \mathcal{M}_{k-1} and \mathcal{M}_k over a shared noise manifold. Specifically, given the current samples $(x_t^k, y^k) \sim p^k$ from task \mathcal{T}_k and the replayed samples $(\hat{x}_t^k, \hat{y}^k) \sim \mathcal{B}_k$, the \mathcal{L}_{IKC} is defined as:

$$\mathcal{L}_{IKC} = \mathbb{E}_{\hat{x}_t^k, \hat{y}^k, x_t^k, y^k, t} [D_\varphi(\epsilon_{\theta_{k-1}}(\hat{x}_t^k, \hat{y}^k, t) \parallel \epsilon_{\theta_k}(x_t^k, y^k, t))], \quad (7)$$

where D_φ is an adaptation via local Bregman divergence minimization with curvature matrix φ .

Crucially, we generalize the conventional squared ℓ_2 distance to a curvature-aware Bregman divergence, defined via a locally-varying positive definite matrix φ that reflects the geometry of the score function landscape.

$$D_\varphi(u \parallel v) = \frac{1}{2}(u - v)^\top \varphi(\hat{x}_t^k, \hat{y}^k, t)(u - v). \quad (8)$$

The preconditioner $\varphi(\hat{x}_t^k, \hat{y}^k, t)$ is derived from the data space metric of \mathcal{M}_{k-1} :

$$\varphi(\hat{x}_t^k, \hat{y}^k, t) = \mathbb{E} \left[\nabla_{\hat{x}_t^k} \log \epsilon_{\theta_{k-1}}(\hat{x}_t^k | \hat{y}^k, t) \times \nabla_{\hat{x}_t^k} \log \epsilon_{\theta_{k-1}}(\hat{x}_t^k | \hat{y}^k, t)^\top \right]. \quad (9)$$

By aligning the divergence metric with the gradient information, which captures the curvature of the teacher model’s parameters \mathcal{M}_{k-1} , the student model \mathcal{M}_k maintains high consistency with its built-in knowledge, effectively reducing the knowledge gap between the two models in Eq. 2.

3.4 Unconditional Knowledge Consistency

Building upon the inter-task model alignment established in Section 3.3, we now operationalize the \mathcal{L}_{UKC} term from Theorem 1, which governs consistency in the mean of unconditional sample embeddings and reverse-time denoising trajectories. This component bridges theoretical bounds with practical implementation by explicitly aligning the mean functions of reverse processes across tasks.

In CDG, deriving task-specific reverse mean functions presents a fundamental challenge. Given current instances $(x_0^k, y^k) \sim (p^k \cup \mathcal{B}_k)$ ⁶ and buffered historical samples $(\hat{x}_0^k, \hat{y}^k) \sim \mathcal{B}_k$, direct computation of $\mathbb{E}[x_t]$ remains ill-posed due to the artificial noise-driven construction of x_t in diffusion frameworks. This arises from the intrinsic semantic mismatch in perturbed diffused states x_t across training phases, rendering naive trajectory averaging and constraint imposition ineffective for gradient-based optimization. To address this, we devise an indirect mean constraint through symbiotic knowledge transfer between the frozen teacher \mathcal{M}_{k-1} and adaptive student \mathcal{M}_k . By reparameterizing $\mathbb{E}[x_{t-1}]$, we enable full gradient backpropagation while enforcing coherent diffused space constraints. Crucially, label-marginalized computation ensures these constraints govern unconditional generation fidelity. The reverse process mean functions for both historical and current models are derived analytically within the shared data using their respective noise prediction networks:

$$\begin{aligned} \mu_{\theta_k}(x_{t-1}, t-1) &= \frac{1}{\sqrt{\alpha_t}} x_t^k - \frac{1 - \alpha_t}{\sqrt{\alpha_t(1 - \bar{\alpha}_t)}} \epsilon_{\theta_k}(x_t^k, t), \\ \mu_{\theta_{k-1}}(\hat{x}_{t-1}, t-1) &= \frac{1}{\sqrt{\alpha_t}} \hat{x}_t^k - \frac{1 - \alpha_t}{\sqrt{\alpha_t(1 - \bar{\alpha}_t)}} \epsilon_{\theta_{k-1}}(\hat{x}_t^k, t). \end{aligned} \quad (10)$$

Here, $\mu_{\theta_{k-1}}(\cdot)$ and $\mu_{\theta_k}(\cdot)$ are the analytically back-calculated means prescribed by historical and current models.

To enforce unconditional mean consistency across incremental adaptations, we formulate \mathcal{L}_{UKC} as a time-weighted divergence between these mean estimates:

$$\mathcal{L}_{UKC} = \frac{\bar{\alpha}_t^2}{1 - \bar{\alpha}_t^2} \left\| \mu_{\theta_k}(x_{t-1}, t-1) - \mu_{\theta_{k-1}}(\hat{x}_{t-1}, t-1) \right\|_2^2. \quad (11)$$

The weighting term $\frac{\bar{\alpha}_t^2}{1 - \bar{\alpha}_t^2}$ emphasizes alignment during semantically critical mid-diffusion phases, where latent structures transition between noise and meaningful representations. By penalizing deviations in denoising trajectories and the mean of unconditional sample embeddings, this loss enforces constraints that preserve the manifold topology of historical data within the evolving student model \mathcal{M}_k . This mechanism complements the instantaneous model matching strategy outlined in Section 3.3, ensuring both local knowledge coherence and global structural fidelity.

3.5 Label Knowledge Consistency

The label knowledge consistency term, denoted as \mathcal{L}_{LKC} , aims to ensure consistency in the shared semantic part of the label space across original samples. To effectively operationalize this concept, we introduce a label regressor, which is not used for optimizing label classification performance, but rather to explore the semantic similarity between \hat{x}_0 and x_0 in the label space, similar to multi-domain alignment methods [10, 21, 15, 5, 47] in zero-shot learning. Moreover, this approach effectively avoids the singularity of label classification, and can be similarly applied when the prior knowledge

⁶In the UKC term, the primary objective is to preserve geometric constraints and retain knowledge across both historical and current data. In the ensuing subsections, we reinforce this continuity by integrating historical data, thereby treating the current samples as a comprehensive amalgamation of both past and present information.

in diffusion models is in the form of text or other modalities. Let \mathcal{M}_k represent the current model for task \mathcal{T}_k , with the corresponding label regressor h_ϕ^k that adapts to the task-specific distribution. The label regressor from the previous task, \mathcal{M}_{k-1} , is frozen to retain the semantic structure of earlier tasks and is represented by the label regressor $h_\phi^{<k}$. Within this framework, we ideally generate samples from $p_t(x_0|x_t)$, i.e., the previous task, to obtain $\hat{x}'_0 = \mathcal{M}_{k-1}(\epsilon, \hat{y}, T)$. However, such sampling incurs substantial computational overhead and resource consumption. Moreover, in \mathcal{M}_{k-1} , the generated images are often nearly indistinguishable from the original ones, rendering explicit sampling redundant. Thus, for efficiency considerations, we directly sample \hat{x}_0 from \mathcal{B}_k to serve as the generated samples, which are then used alongside the current samples x_0 to compute \mathcal{L}_{LKC} .

$$\mathcal{L}_{LKC} = \frac{\bar{\alpha}_t}{\bar{\beta}_t} \mathbb{E}_{\hat{x}_0 \sim \mathcal{B}_k} \left[D_{\text{KL}} \left(h_\phi^{<k}(y|\hat{x}_0) \parallel h_\phi^k(y|x_0) \right) \right]. \quad (12)$$

This objective promotes semantic consistency between historical and current samples by extracting shared prior knowledge, thereby mitigating drift within the label space. Ultimately, through the integration of all three optimization strategies, diffusion models achieve continuous alignment in model parameters, unconditional mean distributions, and the label space, effectively preserving shared knowledge across continual tasks, thereby achieving improved long-term generative performance.

4 Experiments

4.1 Datasets and Benchmark Characteristics

We conduct comprehensive experiments on four representative vision benchmarks spanning diverse domains. **MNIST** [14] consists of 60,000 training and 10,000 test images spanning 10 handwritten digit classes. In our setting, the dataset is partitioned into 5 disjoint tasks, each comprising a subset of the digit classes. **CIFAR-100** [13] comprises 100 object categories, each containing 600 images. The dataset poses significant challenges for CDG due to its low image resolution and minimal knowledge overlap across tasks. It is partitioned into 10 tasks, each with 10 classes. **Flowers102** [23] consists of 8,189 images from 102 flower species with significant intra-class variance. It is divided into 10 tasks for fine-grained generation evaluation. **CUB-200-2011** [36] offers 11,788 bird images from 200 species with subtle morphological variations, split into 10 tasks. To ensure fairness and maintain consistent GPU memory consumption, all images are uniformly resized to 32×32 .

4.2 Metrics

To establish a rigorous theoretical framework for evaluating CF in CDG, we formulate two orthogonally motivated metrics: Mean Fidelity (MF) as a terminal-state performance quantifier and Incremental Mean Fidelity (IMF) as a long-term evaluation quantifier. Given a temporally ordered task manifold $\{\mathcal{T}_k\}_{k=1}^K$, MF interrogates cross-task generative performance through $\text{MF} = \mathbb{E}_{k \sim [1, K]} [d_{\mathcal{M}}(p_{\text{real}}^k \parallel p_{\text{gen}}^k)]$, where $d_{\mathcal{M}}$ operationalizes a generative quality metric (e.g., FID [7]) between ground-truth and synthesized distributions. Conversely, IMF induces a time-incremental aggregation mechanism: $\text{IMF} = \mathbb{E}_{k \sim [1, K]} [\mathbb{E}_{i \leq k} [d_{\mathcal{M}}(p_{\text{real}}^i \parallel p_{\text{gen}}^i)]]$, formally encoding the expected trajectory stability under sequential updates. This dual-metric paradigm dissects both terminal performance degradation (via MF’s terminal-state evaluation) and streaming generation robustness (through IMF’s incremental analysis). To eliminate confounding factors, we enforce strict experimental controls including fixed-output cardinality (2048 samples) and balanced class-conditioned sampling, ensuring metrological consistency. The proposed metrics establish a comprehensive evaluation protocol for assessing both instance-specific generation fidelity and longitudinal knowledge preservation in non-stationary generative scenarios.

4.3 Experimental Implementation

All investigations are rigorously conducted under identical hardware setups and environmental conditions to eliminate confounding variables. The neural architecture leverages the diffusers library-implemented UNet2DModel with hierarchical residual connections, featuring four stages of downsampling/upsampling blocks (128→256→256→256 channels) where the third downblock and second upblock integrate attention mechanisms. The label regressor is strategically deployed in the penultimate feature space to mitigate interference from raw noise patterns. A uniform learning rate of

Table 1: A comprehensive performance comparison across various buffer configurations and methodologies is conducted, ensuring that all experiments are executed under identical hardware setups and environmental conditions to maintain fairness and reproducibility.

Method	MNIST-5T		CIFAR100-10T		Flowers102-10T		CUB200-10T		Average	
	MF (\downarrow)	IMF (\downarrow)	MF (\downarrow)	IMF (\downarrow)	MF (\downarrow)	IMF (\downarrow)	MF (\downarrow)	IMF (\downarrow)	MF (\downarrow)	IMF (\downarrow)
Non-CL	4.99	4.99	65.97	65.97	21.16	21.16	35.80	35.80	31.98	31.98
Rehearsal-free Methods										
KD	62.83	58.98	114.22	103.40	102.49	117.79	157.70	111.07	109.31	97.81
EWC	119.29	176.59	110.07	141.78	104.91	114.35	165.19	163.08	124.86	148.95
L2	105.34	67.66	134.25	129.48	153.53	132.70	125.47	108.61	129.65	109.61
SI	85.39	66.95	145.06	132.67	148.00	136.80	142.90	132.01	130.34	117.11
MAS	291.70	304.40	146.77	169.19	104.99	317.51	128.66	154.84	168.03	236.48
C-LoRA	106.71	80.63	134.58	131.47	369.62	363.88	142.85	129.43	188.44	176.35
Storage Rehearsal Methods (buffer=512)										
ER	97.57	69.38	94.19	89.30	88.36	94.06	130.57	135.07	102.67	96.95
A-GEM	94.67	66.00	96.85	90.80	89.41	92.59	121.73	139.66	100.66	97.26
CCD (Ours)	79.76	57.63	96.34	90.14	86.11	92.18	121.15	101.42	95.84	85.34
Storage Rehearsal Methods (buffer=2560)										
ER	73.60	56.95	103.38	98.55	67.89	80.33	373.50	353.32	154.59	147.29
A-GEM	69.77	54.32	104.58	99.43	66.36	79.79	103.78	114.93	86.12	87.12
CCD (Ours)	67.48	50.94	101.51	98.68	65.31	79.70	106.93	84.11	85.31	78.36
Storage Rehearsal Methods (buffer=5120)										
ER	60.40	135.19	103.34	99.39	67.19	80.23	135.98	164.87	91.73	119.92
A-GEM	68.59	107.24	103.87	100.49	65.39	79.71	70.33	99.21	77.05	96.66
CCD (Ours)	48.97	40.08	102.09	98.33	64.97	79.62	67.00	61.37	70.76	69.85

$1e-3$ is systematically applied across all trials, coupled with the Adam optimizer for optimization. To ensure an absolutely equitable experimental framework, identical training epochs, batch sizes, and dataset partitioning strategies are meticulously maintained for each benchmark dataset. The complete experimental protocol is executed on four NVIDIA A100-40G GPU accelerators. For a more detailed model architecture diagram, please refer to Appendix C.

4.4 Performance Comparison

In Tab. 1, we integrate classification-inspired CL methods into the CDG setting, executing a comprehensive study of their continual generative efficacy. Our evaluation spans established CL methods including Knowledge Distillation (KD) [8], Elastic Weight Consolidation (EWC) [12], L2 Regularization [29], Synaptic Intelligence (SI) [45], Memory-Aware Synapses (MAS) [2], Continual-LoRA (C-LoRA) [30], Experience Replay (ER) [18], and Averaged-Gradient Episodic Memory (A-GEM) [4]. Interestingly, our evaluation reveals that even stable diffusion models suffer from generative collapse under standard CL regimes, resembling GAN instabilities, particularly on the CUB and Flowers102 benchmarks. This underscores the urgent need for a foundational re-evaluation of CDG methods before advancing novel techniques. To this end, we systematically dissect classical paradigms, establishing essential baselines for this emerging research frontier.

Experimental results demonstrate that our method achieves substantial performance gains on the MNIST and CUB200 datasets, with the IMF metric showing marked superiority over ER [18] and A-GEM [4] across all buffer size configurations. This strong empirical evidence confirms that our CCD framework enables stable and high-quality continual generation in CDG, particularly on datasets with high inter-task knowledge overlap, while effectively mitigating the CF phenomenon. On the Flowers102 dataset, which contains relatively few training samples and permits the buffer to store a representative portion of the data, our method maintains a consistent, though moderate, advantage over baseline approaches. However, the performance gap is less pronounced compared to MNIST and CUB200. As anticipated, results on the CIFAR100 dataset are less favorable, with some metrics underperforming relative to traditional ER [18]. This limitation likely stems from the low inter-task

knowledge correlation inherent in coarse-grained datasets, where minimal shared knowledge across tasks renders aggressive retention strategies counterproductive, potentially impairing future generative performance. This finding highlights a key open challenge for future research: *developing effective strategies for knowledge retention and propagation under conditions of minimal cross-task overlap*.

Collectively, our CCD framework achieves state-of-the-art performance across three benchmark datasets, excluding CIFAR100, delivering substantial average improvements in both MF and IMF metrics under all three buffer size configurations. Moreover, the training process remains notably stable, with no observed instances of cross-task generative collapse. These results offer foundational insights and practical guidance for advancing continual data generation, particularly in addressing the stability challenges unique to sequential generative model training. To further illustrate the effectiveness of our approach, we present visualizations of samples generated for the first task at the final training stage in Appendix D. These qualitative results provide a more intuitive and direct assessment of generative retention compared to numerical metrics.

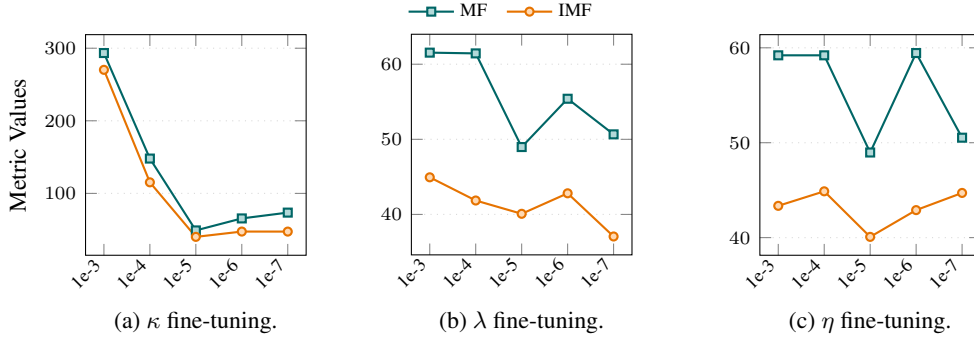


Figure 2: Hyperparameter sensitivity analysis on the MNIST dataset, illustrating the effects of fine-tuning κ , λ , and η on the metrics for MF and IMF.

4.5 Hyperparameter Fine-tuning

In this subsection, we conduct comprehensive hyperparameter tuning experiments associated with Eq. 1, using the MNIST dataset as the evaluation benchmark. Our sensitivity analysis (Fig. 2) highlights the pivotal role of three interrelated hyperparameters, κ , λ , and η , whose interplay governs CDG performance. The model consistency coefficient κ achieves optimal MF and IMF scores (48.97 and 40.08) at 1×10^{-5} . Increasing κ to 1×10^{-3} significantly elevates MF (up to 293.36), suggesting overreliance on prior models, while reducing it to 1×10^{-7} causes a 18.2% drop in IMF, reflecting insufficient consistency. These trends show that moderate temporal coherence is essential for balancing adaptability and retention. The unconditional knowledge consistency weight λ shows a similarly sensitive effect. At 1×10^{-5} , IMF is minimized, whereas increasing it to 1×10^{-3} degrades IMF by 12.1%, indicating that overly strict constraints on the mean of unconditional sample embeddings may impede denoising flexibility. This underscores the importance of calibrated generative invariance. The label knowledge consistency coefficient η also peaks at 1×10^{-5} , effectively preserving cross-task semantic structure in the label space. These results confirm the utility of label-aware consistency in enhancing alignment in CDG and highlight the delicate yet critical balance among the components of our CCD framework. Each hyperparameter contributes uniquely to mitigating CF, and their joint calibration is essential for sustained CDG performance.

4.6 Ablation Studies

To systematically disentangle the contributions of each proposed loss component, we conduct controlled ablation studies on the MNIST benchmark (Tab. 2). The baseline model (MF: 67.60, IMF: 48.79) exhibits substantial forgetting, underscoring the vulnerability of unconstrained diffusion

Table 2: Ablations on each loss component.

Method	MNIST	
	MF (\downarrow)	IMF (\downarrow)
Effect of Removing Individual Loss Components		
Baseline	67.60	48.79
\mathcal{L}_{IKC}	57.92	45.46
$\mathcal{L}_{IKC} + \mathcal{L}_{UKC}$	56.73	38.08
$\mathcal{L}_{IKC} + \mathcal{L}_{LKC}$	50.70	43.79
$\mathcal{L}_{IKC} + \mathcal{L}_{UKC} + \mathcal{L}_{LKC}$	48.97	40.08

trajectories to knowledge drift across tasks. Introducing the inter-task knowledge consistency loss \mathcal{L}_{IKC} significantly improves both metrics (MF: 57.92, IMF: 45.46), demonstrating the importance of Bregman-aligned model consistency in stabilizing forward diffusion dynamics. Adding the unconditional knowledge consistency loss \mathcal{L}_{UKC} further improves performance (MF: 56.73, IMF: 38.08), indicating that aligning the mean of unconditional sample embeddings helps preserve reverse-time denoising trajectories. Substituting \mathcal{L}_{UKC} with the label knowledge consistency loss \mathcal{L}_{LKC} yields stronger gains in MF (50.70) but a smaller improvement in IMF (43.79), suggesting that label-space constraints are particularly effective for preserving shared semantics across tasks. When all three components are combined, the model achieves the best overall performance (MF: 48.97, IMF: 40.08), supporting our central hypothesis that multi-level consistency is critical for mitigating CF in CDG.

5 Conclusion

This work introduces a principled framework for Continual Diffusion Generation (CDG), grounded in stochastic calculus, to tackle catastrophic forgetting (CF) in diffusion models. We characterize forgetting as misalignment in cross-task stochastic differential equation (SDE) dynamics and define three key consistency bounds, inter-task, unconditional mean, and label-level, to ensure stable knowledge retention. Based on these, we propose the Continual Consistency Diffusion (CCD) framework, which enforces multi-scale consistency via hierarchical loss functions that preserve the geometric and semantic integrity of generative trajectories. Experiments across diverse benchmarks show that CCD achieves state-of-the-art results in both Mean Fidelity (MF) and Incremental Mean Fidelity (IMF). By bridging static diffusion models and real-world streaming tasks, this work establishes CDG as a foundation for continual generative modeling in dynamic environments.

References

- [1] Munsif Ali, Leonardo Rossi, and Massimo Bertozzi. Cfts-gan: Continual few-shot teacher student for generative adversarial networks. In *International Conference on Pattern Recognition*, pages 249–262. Springer, 2025.
- [2] Rahaf Aljundi, Francesca Babiloni, Mohamed Elhoseiny, Marcus Rohrbach, and Tinne Tuytelaars. Memory aware synapses: Learning what (not) to forget. In *Proceedings of the European Conference on Computer Vision*, pages 139–154, 2018.
- [3] Brian DO Anderson. Reverse-time diffusion equation models. *Stochastic Processes and their Applications*, 12(3):313–326, 1982.
- [4] Arslan Chaudhry, Marc’Aurelio Ranzato, Marcus Rohrbach, and Mohamed Elhoseiny. Efficient lifelong learning with a-gem. In *International Conference on Learning Representations*, 2019.
- [5] Bowen Duan, Shiming Chen, Yufei Guo, Guo-Sen Xie, Weiping Ding, and Yisong Wang. Visual-semantic graph matching net for zero-shot learning. *IEEE Transactions on Neural Networks and Learning Systems*, 2024.
- [6] Yi Gu, Jie Li, Yuting Gao, Ruoxin Chen, Chentao Wu, Feiyang Cai, Chao Wang, and Zirui Zhang. Association: Remind your gan not to forget. *arXiv preprint arXiv:2011.13553*, 2020.
- [7] Martin Heusel, Hubert Ramsauer, Thomas Unterthiner, Bernhard Nessler, and Sepp Hochreiter. Gans trained by a two time-scale update rule converge to a local nash equilibrium. *Advances in neural information processing systems*, 30, 2017.
- [8] Geoffrey Hinton. Distilling the knowledge in a neural network. *arXiv preprint arXiv:1503.02531*, 2015.
- [9] Jonathan Ho, Ajay Jain, and Pieter Abbeel. Denoising diffusion probabilistic models. *Advances in Neural Information Processing Systems*, 33:6840–6851, 2020.
- [10] Sung Ju Hwang and Leonid Sigal. A unified semantic embedding: Relating taxonomies and attributes. *Advances in Neural Information Processing Systems*, 27, 2014.

- [11] Dahuin Jung, Dongyoon Han, Jihwan Bang, and Hwanjun Song. Generating instance-level prompts for rehearsal-free continual learning. In *Proceedings of the IEEE/CVF International Conference on Computer Vision*, pages 11847–11857, 2023.
- [12] James Kirkpatrick, Razvan Pascanu, Neil Rabinowitz, Joel Veness, Guillaume Desjardins, Andrei A Rusu, Kieran Milan, John Quan, Tiago Ramalho, Agnieszka Grabska-Barwinska, et al. Overcoming catastrophic forgetting in neural networks. *Proceedings of the National Academy of Sciences*, 114(13):3521–3526, 2017.
- [13] Alex Krizhevsky and Geoffrey Hinton. Learning multiple layers of features from tiny images. Technical Report 0, University of Toronto, Toronto, Ontario, 2009. URL <https://www.cs.toronto.edu/~kriz/learning-features-2009-TR.pdf>.
- [14] Yann LeCun, Léon Bottou, Yoshua Bengio, and Patrick Haffner. Gradient-based learning applied to document recognition. *Proceedings of the IEEE*, 86(11):2278–2324, 1998.
- [15] Xiaofan Li, Yachao Zhang, Shiran Bian, Yanyun Qu, Yuan Xie, Zhongchao Shi, and Jianping Fan. Vs-boost: Boosting visual-semantic association for generalized zero-shot learning. In *IJCAI*, pages 1107–1115, 2023.
- [16] Zhizhong Li and Derek Hoiem. Learning without forgetting. *IEEE Transactions on Pattern Analysis and Machine Intelligence*, 40(12):2935–2947, 2017.
- [17] Jingren Liu, Zhong Ji, YunLong Yu, Jiale Cao, Yanwei Pang, Jungong Han, and Xuelong Li. Parameter-efficient fine-tuning for continual learning: A neural tangent kernel perspective. *arXiv preprint arXiv:2407.17120*, 2024.
- [18] David Lopez-Paz and Marc’Aurelio Ranzato. Gradient episodic memory for continual learning. *Advances in Neural Information Processing Systems*, 30, 2017.
- [19] Cheng Lu, Yuhao Zhou, Fan Bao, Jianfei Chen, Chongxuan Li, and Jun Zhu. Dpm-solver: A fast ode solver for diffusion probabilistic model sampling in around 10 steps. *Advances in Neural Information Processing Systems*, 35:5775–5787, 2022.
- [20] Sergi Masip, Pau Rodriguez, Tinne Tuytelaars, and Gido M van de Ven. Continual learning of diffusion models with generative distillation. *arXiv preprint arXiv:2311.14028*, 2023.
- [21] Jian Ni, Shanghang Zhang, and Haiyong Xie. Dual adversarial semantics-consistent network for generalized zero-shot learning. *Advances in neural information processing systems*, 32, 2019.
- [22] Alexander Quinn Nichol and Prafulla Dhariwal. Improved denoising diffusion probabilistic models. In *International Conference on Machine Learning*, pages 8162–8171. PMLR, 2021.
- [23] Maria-Elena Nilsback and Andrew Zisserman. Automated flower classification over a large number of classes. In *2008 Sixth Indian Conference on Computer Vision, Graphics & Image Processing*, pages 722–729. IEEE, 2008.
- [24] German I Parisi, Ronald Kemker, Jose L Part, Christopher Kanan, and Stefan Wermter. Continual lifelong learning with neural networks: A review. *Neural Networks*, 113:54–71, 2019.
- [25] Benedikt Pflüß, Alexander Gepperth, and Benedikt Bagus. Continual learning with fully probabilistic models. *arXiv preprint arXiv:2104.09240*, 2021.
- [26] David Rolnick, Arun Ahuja, Jonathan Schwarz, Timothy Lillicrap, and Gregory Wayne. Experience replay for continual learning. *Advances in Neural Information Processing Systems*, 32, 2019.
- [27] Ali Siahkamari, Xide Xia, Venkatesh Saligrama, David Castañón, and Brian Kulis. Learning to approximate a bregman divergence. *Advances in Neural Information Processing Systems*, 33: 3603–3612, 2020.
- [28] James Seale Smith, Leonid Karlinsky, Vyshnavi Gutta, Paola Cascante-Bonilla, Donghyun Kim, Assaf Arbelle, Rameswar Panda, Rogerio Feris, and Zsolt Kira. Coda-prompt: Continual decomposed attention-based prompting for rehearsal-free continual learning. In *Proceedings of the IEEE/CVF Conference on Computer Vision and Pattern Recognition*, pages 11909–11919, 2023.

- [29] James Seale Smith, Junjiao Tian, Shaunak Halbe, Yen-Chang Hsu, and Zsolt Kira. A closer look at rehearsal-free continual learning. In *Proceedings of the IEEE/CVF Conference on Computer Vision and Pattern Recognition*, pages 2410–2420, 2023.
- [30] James Seale Smith, Yen-Chang Hsu, Lingyu Zhang, Ting Hua, Zsolt Kira, Yilin Shen, and Hongxia Jin. Continual diffusion: Continual customization of text-to-image diffusion with c-lora. *arXiv preprint arXiv:2304.06027*, 2024.
- [31] Jiaming Song, Chenlin Meng, and Stefano Ermon. Denoising diffusion implicit models. *arXiv preprint arXiv:2010.02502*, 2020.
- [32] Yang Song, Jascha Sohl-Dickstein, Diederik P Kingma, Abhishek Kumar, Stefano Ermon, and Ben Poole. Score-based generative modeling through stochastic differential equations. In *International Conference on Learning Representations*, 2021.
- [33] Gan Sun, Wenqi Liang, Jiahua Dong, Jun Li, Zhengming Ding, and Yang Cong. Create your world: Lifelong text-to-image diffusion. *IEEE Transactions on Pattern Analysis and Machine Intelligence*, 2024.
- [34] Sakshi Varshney, Vinay Kumar Verma, PK Srijith, Lawrence Carin, and Piyush Rai. Camgan: Continual adaptation modules for generative adversarial networks. *Advances in Neural Information Processing Systems*, 34:15175–15187, 2021.
- [35] Pascal Vincent. A connection between score matching and denoising autoencoders. *Neural Computation*, 23(7):1661–1674, 2011.
- [36] Catherine Wah, Steve Branson, Peter Welinder, Pietro Perona, and Serge Belongie. The Caltech-UCSD Birds-200-2011 Dataset. Technical Report CNS-TR-2011-001, California Institute of Technology, 2011.
- [37] Liyuan Wang, Jingyi Xie, Xingxing Zhang, Mingyi Huang, Hang Su, and Jun Zhu. Hierarchical decomposition of prompt-based continual learning: Rethinking obscured sub-optimality. *Advances in Neural Information Processing Systems*, 36, 2024.
- [38] Yabin Wang, Zhiwu Huang, and Xiaopeng Hong. S-prompts learning with pre-trained transformers: An occam’s razor for domain incremental learning. *Advances in Neural Information Processing Systems*, 35:5682–5695, 2022.
- [39] Zifeng Wang, Zizhao Zhang, Sayna Ebrahimi, Ruoxi Sun, Han Zhang, Chen-Yu Lee, Xiaoqi Ren, Guolong Su, Vincent Perot, Jennifer Dy, et al. Dualprompt: Complementary prompting for rehearsal-free continual learning. In *European Conference on Computer Vision*, pages 631–648. Springer, 2022.
- [40] Zifeng Wang, Zizhao Zhang, Chen-Yu Lee, Han Zhang, Ruoxi Sun, Xiaoqi Ren, Guolong Su, Vincent Perot, Jennifer Dy, and Tomas Pfister. Learning to prompt for continual learning. In *Proceedings of the IEEE/CVF Conference on Computer Vision and Pattern Recognition*, pages 139–149, 2022.
- [41] Fei Ye and Adrian G Bors. Lifelong twin generative adversarial networks. In *IEEE International Conference on Image Processing*, pages 1289–1293. IEEE, 2021.
- [42] Fei Ye and Adrian G Bors. Lifelong teacher-student network learning. *IEEE Transactions on Pattern Analysis and Machine Intelligence*, 44(10):6280–6296, 2021.
- [43] Jason Yoo, Yingchen He, Saeid Naderiparizi, Dylan Green, Gido M. van de Ven, Geoff Pleiss, and Frank Wood. Lifelong learning of video diffusion models from a single video stream, 2024. URL <https://arxiv.org/abs/2406.04814>.
- [44] Tianhe Yu, Saurabh Kumar, Abhishek Gupta, Sergey Levine, Karol Hausman, and Chelsea Finn. Gradient surgery for multi-task learning. *Advances in Neural Information Processing Systems*, 33:5824–5836, 2020.
- [45] Friedemann Zenke, Ben Poole, and Surya Ganguli. Continual learning through synaptic intelligence. In *International Conference on Machine Learning*, pages 3987–3995. PMLR, 2017.

- [46] Haotian Zhang, Junting Zhou, Haowei Lin, Hang Ye, Jianhua Zhu, Zihao Wang, Liangcai Gao, Yizhou Wang, and Yitao Liang. Clog: Benchmarking continual learning of image generation models. *arXiv preprint arXiv:2406.04584*, 2024.
- [47] Sheng Zhang, Muzammal Naseer, Guangyi Chen, Zhiqiang Shen, Salman Khan, Kun Zhang, and Fahad Shahbaz Khan. S3a: Towards realistic zero-shot classification via self structural semantic alignment. In *Proceedings of the AAAI Conference on Artificial Intelligence*, volume 38, pages 7278–7286, 2024.
- [48] Xiaochen Zhao, Jingxiang Sun, Lizhen Wang, Jinli Suo, and Yebin Liu. Invertavatar: Incremental gan inversion for generalized head avatars. In *ACM SIGGRAPH 2024 Conference Papers*, pages 1–10, 2024.
- [49] Kaiwen Zheng, Cheng Lu, Jianfei Chen, and Jun Zhu. Dpm-solver-v3: Improved diffusion ode solver with empirical model statistics. *Advances in Neural Information Processing Systems*, 36: 55502–55542, 2023.
- [50] Da-Wei Zhou, Hai-Long Sun, Han-Jia Ye, and De-Chuan Zhan. Expandable subspace ensemble for pre-trained model-based class-incremental learning. In *Proceedings of the IEEE/CVF Conference on Computer Vision and Pattern Recognition*, pages 23554–23564, 2024.

A Preliminaries in SDE Diffusion Models

In this section, we introduce key preliminary concepts essential for the theoretical derivations that follow. Specifically, we discuss the framework of Stochastic Differential Equations (SDEs) and establish their equivalence with Denoising Diffusion Probabilistic Models (DDPMs), highlighting their shared formulation in modeling diffusion processes. This correspondence demonstrates that SDEs and DDPMs can be treated interchangeably in certain contexts.

A.1 Fundamental Concepts

Within the framework of stochastic differential equations (SDEs), controllable diffusion models are utilized to model the temporal evolution of data states under specified conditions or labels. Let x_t denote the data state at time t . The forward SDE is defined as:

$$dx_t = f(x_t, t) dt + g(t) dW_t, \quad (13)$$

where $f(x_t, t)$ represents the drift term, and $g(t)$ signifies the diffusion coefficient. Here, W_t is a standard Wiener process (standard Brownian motion).

By incorporating the Fokker-Planck equation and reverse-time dynamics in [3, 32], the corresponding reverse SDE can be formulated with an additional drift adjustment:

$$dx_t = (f(x_t, t) - g^2(t) \nabla_{x_t} \log p_t(x_t|y)) dt + g(t) dW_t, \quad (14)$$

where the additional term $\nabla_{x_t} \log p_t(x_t|y)$ corresponds to the gradient of the log-probability of the conditional distribution $p_t(x_t|y) = p(x_t|y, t)$. Direct computation of this gradient is often infeasible for high-dimensional data and is thus typically approximated using a score estimator ϵ_θ .

The score estimator ϵ_θ is employed to approximate the required $\nabla_{x_t} \log p_t(x_t)$ for unconditional diffusion generation, and the optimization is achieved through the following loss function:

$$\epsilon_\theta^* = \arg \min_{\theta} \mathbb{E}_t \left\{ \lambda(t) \mathbb{E}_{p(x_0)} \mathbb{E}_{p(x_t|x_0)} [\|\epsilon_\theta(x_t, t) - \nabla_{x_t} \log p(x_t|x_0)\|_2^2] \right\}. \quad (15)$$

Here, $\lambda : [0, T] \in \mathbb{R}_{>0}$ is a positive weighting function, t is uniformly sampled over $[0, T]$, $x_0 \sim p(x_0)$ and $x_t \sim p(x_t|x_0)$. With adequate data and sufficient model capacity, score matching ensures that the optimal solution to Eq. 15, denoted by ϵ_θ^* , equals $\nabla_{x_t} \log p_t(x_t)$ for almost all x and t .

To utilize the unconditional generation's ϵ_θ^* to obtain the optimal parameters for conditional generation, we use $p_t(x_t|y) = \frac{p_t(x_t, y)}{p_t(y)}$ to derive $\nabla_{x_t} \log p_t(x_t|y) = \nabla_{x_t} \log p_t(x_t, y) - \nabla_{x_t} \log p_t(y)$. Since $p_t(y)$ does not depend on x_t , we have $\nabla_{x_t} \log p_t(x_t|y) = \nabla_{x_t} \log p_t(x_t, y)$. Next, by the chain rule of differentiation, the gradient of the joint log-probability can be written as:

$$\nabla_{x_t} \log p_t(x_t|y) = \nabla_{x_t} \log p_t(x_t) + \nabla_{x_t} \log p_t(y|x_t) = \epsilon_\theta^* + \nabla_{x_t} \log p_t(y|x_t). \quad (16)$$

A.2 Equivalence Between DDPM and SDE Models

In the Denoising Diffusion Probabilistic Model (DDPM) framework [9, 22], the data evolves through a forward process that progressively adds Gaussian noise to an initial sample x_0 , resulting in a noisy sample x_t . The probability distribution of x_t conditioned on x_0 can be written as:

$$p_t(x_t|x_0) = \mathcal{N}(x_t; \bar{\alpha}_t x_0, \bar{\beta}_t^2 I), \quad (17)$$

where $\bar{\alpha}_t$ and $\bar{\beta}_t$ are time-dependent coefficients that determine the scaling of the original data and the variance of the noise, respectively. Among them, $\bar{\alpha}_t = \sqrt{\prod_{s=1}^t \alpha_s}$ and $\bar{\beta}_t^2 = 1 - \bar{\alpha}_t^2$.

From this, we can express the noisy sample x_t as:

$$x_t = \bar{\alpha}_t x_0 + \bar{\beta}_t \varepsilon, \quad \varepsilon \sim \mathcal{N}(0, I). \quad (18)$$

To recover x_0 from x_t , rearrange the equation:

$$x_0 = \frac{1}{\bar{\alpha}_t} x_t - \frac{\bar{\beta}_t}{\bar{\alpha}_t} \varepsilon. \quad (19)$$

This equation elucidates how x_0 can be estimated from x_t using the scaling factor $\bar{\alpha}_t$ and the noise variance $\bar{\beta}_t$, both of which are determined by the forward process in DDPM.

In the SDE framework, the forward SDE for a Variance Preserving SDE (VP-SDE) is:

$$dx = -\frac{1}{2}\beta(t)x dt + \sqrt{\beta(t)} dW, \quad (20)$$

which has the solution:

$$x_t = e^{-\frac{1}{2} \int_0^t \beta(s) ds} x_0 + \int_0^t \sqrt{\beta(s)} e^{-\frac{1}{2} \int_s^t \beta(u) du} dW_s. \quad (21)$$

By choosing $\bar{\alpha}(t) = e^{-\frac{1}{2} \int_0^t \beta(s) ds}$ and $\bar{\sigma}^2(t) = 1 - \bar{\alpha}^2(t)$, we can write:

$$x_t = \bar{\alpha}(t)x_0 + \bar{\sigma}(t)z, \quad z \sim \mathcal{N}(0, I). \quad (22)$$

In this case, the relationship between x_0 and x_t is:

$$x_0 = \frac{1}{\bar{\alpha}(t)}x_t - \frac{\bar{\sigma}(t)}{\bar{\alpha}(t)}z. \quad (23)$$

This expression mirrors the form derived in the DDPM framework. To ensure consistency between the DDPM and SDE frameworks, we equate the coefficients from both equations. Thus, we have:

$$\bar{\alpha}(t) = \bar{\alpha}_t \quad \text{and} \quad \bar{\sigma}(t) = \bar{\beta}_t. \quad (24)$$

This shows that $\bar{\sigma}(t)$ in the SDE framework can be expressed as $\bar{\beta}_t$ from the DDPM framework when appropriate diffusion coefficients and scaling functions are selected.

A.3 Approximation of Score Functions and Noise Prediction

With the relationship between x_0 and x_t established, we now turn to the connection between the score function in SDEs and the noise prediction model in DDPMs. Certainly, this is merely a rough justification. A more comprehensive and rigorous proof of the equivalence between the two can be found in [35]. In the SDE framework, the score function is defined as the gradient of the log-probability $p_t(x_t|x_0)$ with respect to x_t :

$$\nabla_{x_t} \log p_t(x_t|x_0) = -\frac{1}{\bar{\sigma}(t)^2}(x_t - \bar{\alpha}(t)x_0). \quad (25)$$

Substituting $\bar{\sigma}(t) = \bar{\beta}_t$ and $\bar{\alpha}(t) = \bar{\alpha}_t$, we obtain:

$$\nabla_{x_t} \log p_t(x_t|x_0) = -\frac{1}{\bar{\beta}_t^2}(x_t - \bar{\alpha}_t x_0). \quad (26)$$

In DDPM, the model $\varepsilon_\theta(x_t, t)$ is trained to predict the noise ε , allowing us to express $x_t = \bar{\alpha}_t x_0 + \bar{\beta}_t \varepsilon$.

$$\nabla_{x_t} \log p_t(x_t|x_0) = -\frac{1}{\bar{\beta}_t} \varepsilon_\theta(x_t, t). \quad (27)$$

With a large amount of x_0 training, $\nabla_{x_t} \log p_t(x_t|x_0)$ will approximate $\nabla_{x_t} \log p_t(x_t) = \epsilon_\theta(x_t, t)$. This establishes the connection between the score function in SDEs and the noise prediction model in DDPMs. Consequently, the score estimator $\epsilon_\theta(x_t, t)$ in the SDE framework can be approximated by the noise predictor $\varepsilon_\theta(x_t, t)$ from DDPMs.

$$\epsilon_\theta(x_t, t) = \nabla_{x_t} \log p_t(x_t) \approx \mathbb{E}_{p(x_0), p(x_t|x_0)} [\nabla_{x_t} \log p_t(x_t|x_0)] \approx -\frac{\varepsilon_\theta(x_t, t)}{\bar{\beta}_t}. \quad (28)$$

In summary, we have demonstrated that the relationship between x_0 and x_t in the SDE framework can be expressed similarly to that in the DDPM framework by appropriately selecting the diffusion coefficient $\sigma(t)$ as $\bar{\beta}_t$. Furthermore, the noise prediction model $\varepsilon_\theta(x_t, t)$ in DDPM is approximately equivalent to the score estimator $\epsilon_\theta(x_t, t)$ in the SDE framework, with a scaling factor $\bar{\beta}_t$. This demonstrates the close correspondence between DDPMs and SDEs, and in the subsequent derivations, we will treat them as equivalent processes, having completed the detailed derivation.

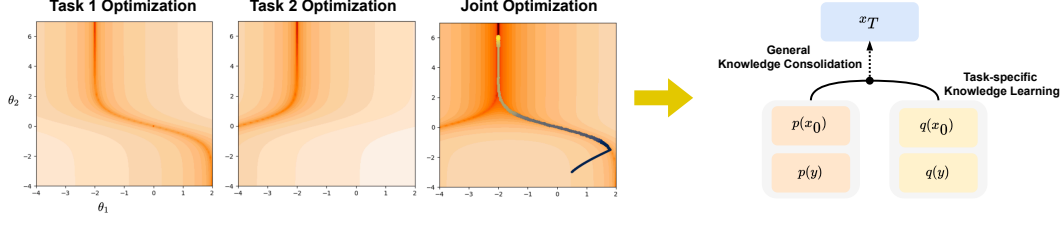


Figure 3: Borrowing from [44], during multi-task optimization, the gradients will eventually converge. Therefore, in a streaming scenario, there exists a portion of shared knowledge, which ensures that $p_t(x_t|x_0, y) = q_t(x_t|x_0, y)$ and $\nabla_{x_t}\mu(x_t, t) \approx \nabla_{x_t}\nu(x_t, t)$. This shared knowledge is crucial for the diffusion generator’s ability to retain and transfer knowledge in continual generation.

B Cross-Task Diffusion Evolution

From a Bayesian perspective, we analyze the forward transfer of diffusion models between two tasks \mathcal{T}_i and \mathcal{T}_j . The visual space distributions of these tasks can be represented as $p(x_0)$ and $q(x_0)$, where x_0 encompasses all visual samples within \mathcal{T}_i and \mathcal{T}_j . The label spaces are expressed as $p(y)$ and $q(y)$, with y representing all labels within \mathcal{T}_i and \mathcal{T}_j . As illustrated in Fig. 3, the relationship between these tasks can be visualized through the joint distribution of $p(x_0, y)$ and $q(x_0, y)$. The task-specific distributions $p(x_0)$ and $q(x_0)$ share certain overlapping regions in the visual space, signifying common knowledge that can be transferred between the tasks. The key challenge is to leverage these shared regions while accounting for task-specific differences in visual and label spaces.

We divide the training objective into two parts. The first part involves using \mathcal{T}_j data to enable the model to acquire task-specific knowledge pertinent to the target task. This is crucial for preventing underfitting on the target task and is referred to as the task-specific knowledge learning process. The second part focuses on retaining knowledge from the source task \mathcal{T}_i . We refer to this process as the common knowledge consolidation process, aimed at preventing overfitting on the target domain and further strengthening the shared knowledge from the source task. This training strategy not only helps the model adapt better to new tasks but also ensures the effective retention of previously learned shared knowledge. In addition, based on the assumptions, we can establish the optimization relationship between the source and target tasks:

$$\begin{aligned} \log q_t(x_t|y) &= \log \left(\int p_t(x_t|x_0, y) \frac{q_t(x_0|y)}{p_t(x_0|y)} p_t(x_0|y) dx_0 \right) \\ &= \log \left(p_t(x_t|y) \mathbb{E}_{p_t(x_0|x_t, y)} \left[\frac{q_t(x_0|y)}{p_t(x_0|y)} \right] \right) \\ &= \log p_t(x_t|y) + \log \mathbb{E}_{p_t(x_0|x_t, y)} \left[\frac{q_t(x_0|y)}{p_t(x_0|y)} \right], \end{aligned} \quad (29)$$

where $\mathbb{E}_{p_t(x_0|x_t, y)}[\cdot]$ denotes the conditional expectation under the posterior distribution $p_t(x_0|x_t, y)$ given x_t .

To refine this analysis, we compute the gradient of $\log q_t(x_t|y)$ with respect to the data state x_t ⁷:

$$\nabla_{x_t} \log q_t(x_t|y) = \nabla_{x_t} \log p_t(x_t|y) + \mathbb{E}_{p_t(x_0|x_t, y)} \left[\nabla_{x_t} \log \frac{q_t(x_0|y)}{p_t(x_0|y)} \right]. \quad (30)$$

Since \mathcal{T}_i and \mathcal{T}_j share some overlapping knowledge, we directly perform differential calculations on x_t . The key quantity of interest is the term $\nabla_{x_t} \log \mathbb{E}_{p_t(x_0|x_t, y)} \left[\frac{q_t(x_0|y)}{p_t(x_0|y)} \right]$, which can be expressed as the difference in noise terms between the tasks. And further combining with Eq. 16, we obtain:

$$\epsilon_\theta^q - \epsilon_\theta^p = \nabla_{x_t} \log \mathbb{E}_{p_t(x_0|x_t, y)} \left[\frac{q_t(x_0|y)}{p_t(x_0|y)} \right] + \nabla_{x_t} \log \frac{p_t(y|x_t)}{q_t(y|x_t)}, \quad (31)$$

where ϵ_θ^q and ϵ_θ^p represent the noise approximations for tasks \mathcal{T}_j and \mathcal{T}_i , respectively.

⁷ x_t represents the shared knowledge in the p and q , rather than diffused samples from a single distribution.

To achieve a simplified formulation, we employ Jensen’s inequality, assuming equivalence between the conditional distributions of the original and synthesized imagery, i.e., $p_t(x_0|x_t, y) = p_t(x_0|y)$ and $q_t(x_0|x_t, y) = q_t(x_0|y)$. This alignment facilitates the derivation of a computationally amenable lower bound through the interchange of the logarithmic operation with the expectation:

$$\begin{aligned} & \nabla_{x_t} \log \mathbb{E}_{p_t(x_0|x_t, y)} \left[\frac{q_t(x_0|y)}{p_t(x_0|y)} \right] \\ & \geq \mathbb{E}_{p_t(x_0|x_t, y)} \left[\nabla_{x_t} \log \frac{q_t(x_0|y)}{p_t(x_0|y)} \right] \\ & \approx -\nabla_{x_t} D_{KL} \left(p_t(x_0|x_t, y) \parallel q_t(x_0|x_t, y) \right). \end{aligned} \quad (32)$$

where D_{KL} denotes the Kullback-Leibler (KL) divergence between the posteriors.

Finally, we re-express the gradient relationship as:

$$\begin{aligned} & \epsilon_\theta^q - \epsilon_\theta^p - \nabla_{x_t} \log \mathbb{E}_{p_t(x_0|x_t, y)} \left[\frac{q_t(x_0|y)}{p_t(x_0|y)} \right] + \nabla_{x_t} \log \frac{q_t(y|x_t)}{p_t(y|x_t)} \\ & \leq \epsilon_\theta^q - \epsilon_\theta^p + \nabla_{x_t} D_{KL} \left(p_t(x_0|x_t, y) \parallel q_t(x_0|x_t, y) \right) + \nabla_{x_t} \log \frac{q_t(y|x_t)}{p_t(y|x_t)}. \end{aligned} \quad (33)$$

Thus, the evolution of cross-task diffusion can be systematically characterized through the gradient of the KL divergence, offering a principled framework to govern the conditional diffusion process across tasks. This framework not only ensures the fidelity of the generated samples to their respective tasks but also captures the intrinsic inter-task relationship in a mathematically coherent manner.

Applying Bayes’ theorem to decompose $p_t(x_0|x_t, y)$, we obtain $p_t(x_0|x_t, y) = \frac{p_t(x_0|x_t)p_t(y|x_0)}{p_t(y|x_t)}$. Similarly, by performing an analogous decomposition for $q_t(x_0|x_t, y)$, we arrive at:

$$\begin{aligned} & \nabla_{x_t} D_{KL} \left(p_t(x_0|x_t, y) \parallel q_t(x_0|x_t, y) \right) \\ & = \nabla_{x_t} \int p_t(x_0|x_t, y) \log \frac{\frac{p_t(x_0|x_t)p_t(y|x_0)}{p_t(y|x_t)}}{\frac{q_t(x_0|x_t)q_t(y|x_0)}{q_t(y|x_t)}} dx_0 \\ & = \nabla_{x_t} \int p_t(x_0|x_t, y) \left[\log \frac{p_t(x_0|x_t)}{q_t(x_0|x_t)} + \log \frac{p_t(y|x_0)}{q_t(y|x_0)} + \log \frac{q_t(y|x_t)}{p_t(y|x_t)} \right] dx_0 \\ & = \nabla_{x_t} \int p_t(x_0|x_t, y) \log \frac{p_t(x_0|x_t)}{q_t(x_0|x_t)} dx_0 \\ & \quad + \nabla_{x_t} \int p_t(x_0|x_t, y) \log \frac{p_t(y|x_0)}{q_t(y|x_0)} dx_0 \\ & \quad + \nabla_{x_t} \log \frac{q_t(y|x_t)}{p_t(y|x_t)} \int p_t(x_0|x_t, y) dx_0 \\ & = \underbrace{\nabla_{x_t} \int \frac{p_t(x_0|x_t)p_t(y|x_0)}{p_t(y|x_t)} \log \frac{p_t(x_0|x_t)}{q_t(x_0|x_t)} dx_0}_{\text{Unconditional Knowledge Consistency}} \\ & \quad + \underbrace{\nabla_{x_t} \int \frac{p_t(x_0|x_t)p_t(y|x_0)}{p_t(y|x_t)} \log \frac{p_t(y|x_0)}{q_t(y|x_0)} dx_0}_{\text{Label Knowledge Consistency}} \\ & \quad + \underbrace{\nabla_{x_t} \log \frac{q_t(y|x_t)}{p_t(y|x_t)}}_{\text{Simplifiable Aspect}}. \end{aligned} \quad (34)$$

For the unconditional knowledge consistency term, we assume that, aside from the clean sample x_0 itself, the correlation between y and most diffused samples x_t diminishes as the diffusion process

adds noise. Furthermore, we intentionally avoid introducing an explicit classifier that couples x_t with y . Under this formulation, $p_t(y|x_t)$ can be regarded as irrelevant to the differentiation variable x_t , and $p_t(y|x_0)$ can be reformulated as an external expectation term. Consequently, the unconditional knowledge consistency term simplifies to:

$$\begin{aligned} \nabla_{x_t} \int \frac{p_t(x_0|x_t)p_t(y|x_0)}{p_t(y|x_t)} \log \frac{p_t(x_0|x_t)}{q_t(x_0|x_t)} dx_0 &\propto \nabla_{x_t} \int p_t(x_0|x_t) \log \frac{p_t(x_0|x_t)}{q_t(x_0|x_t)} dx_0 \\ &= \nabla_{x_t} D_{\text{KL}}(p_t(x_0|x_t) \parallel q_t(x_0|x_t)). \end{aligned} \quad (35)$$

Hence, only the gradient of the KL divergence between the two posteriors $p_t(x_0|x_t)$ and $q_t(x_0|x_t)$ remains relevant to optimization, while the label-related factors play no direct role.

In the context of unconditional diffusion generation, both the generative distribution $p(x_0|x_t)$ and the approximate posterior $q(x_0|x_t)$ are typically modeled as Gaussian distributions of the form $\mathcal{N}(x_0; \mu(x_t, t), \sigma_t^2 I)$ and $\mathcal{N}(x_0; \nu(x_t, t), \sigma_t^2 I)$, respectively. The Kullback–Leibler (KL) divergence between these two Gaussians, which share the same isotropic variance $\sigma_t^2 I$, reduces to a simple expression involving their means, namely $D_{\text{KL}} = \frac{(\mu(x_t, t) - \nu(x_t, t))^2}{2\sigma_t^2}$.

Assuming that both $\mu(x_t, t)$ and $\nu(x_t, t)$ are differentiable functions of x_t , and that their dependence on x_t is continuous, we can take the gradient of the KL divergence with respect to x_t . This yields:

$$\nabla_{x_t} D_{\text{KL}} = \frac{(\mu(x_t, t) - \nu(x_t, t))}{\sigma_t^2} (\nabla_{x_t} \mu(x_t, t) - \nabla_{x_t} \nu(x_t, t)) \approx \delta \cdot \frac{\mu(x_t, t) - \nu(x_t, t)}{\sigma_t^2}. \quad (36)$$

where δ represents a small perturbation determined based on the shared knowledge observed in Fig. 3.

Consequently, the term $\nabla_{x_t} D_{\text{KL}}(p_t(x_0|x_t) \parallel q_t(x_0|x_t))$ can be rephrased as:

$$\nabla_{x_t} D_{\text{KL}}(p_t(x_0|x_t) \parallel q_t(x_0|x_t)) = \frac{\bar{\alpha}_t^2}{\bar{\beta}_t^2} [\mu_\theta(x_t, t) - \nu_\theta(x_t, t)]. \quad (37)$$

where $x_0 = \frac{1}{\alpha_t} x_t - \frac{\bar{\beta}_t}{\alpha_t} \varepsilon$, implying that $\sigma_t^2 = \frac{\bar{\beta}_t^2}{\alpha_t^2}$. The parameter θ represents the network parameters utilized in the reparameterization technique to fit the mean. ε is standard normal noise.

Similarly, for the term representing Label Knowledge Consistency, the core focus is on directly describing the differences in the conditional distributions of labels y given x_0 . Here, the labels play a direct comparison role, and the label-related probability distributions directly impact the optimization objective. In contrast, $p_t(y|x_t)$ does not affect the optimization objective related to x_0 and can be neglected to some extent. Therefore, this term can be transformed into:

$$\begin{aligned} &\nabla_{x_t} \int \frac{p_t(x_0|x_t)p_t(y|x_0)}{p_t(y|x_t)} \log \frac{p_t(y|x_0)}{q_t(y|x_0)} dx_0 \\ &\propto \nabla_{x_t} \int p_t(x_0|x_t)p_t(y|x_0) \log \frac{p_t(y|x_0)}{q_t(y|x_0)} dx_0 \\ &= \int \nabla_{x_t} p_t(x_0|x_t)p_t(y|x_0) \log \frac{p_t(y|x_0)}{q_t(y|x_0)} dx_0 \\ &= \mathbb{E}_{\nabla_{x_t} p(x_0|x_t)} [D_{\text{KL}}(p_t(y|x_0) \parallel q_t(y|x_0))]. \end{aligned} \quad (38)$$

In diffusion models, $p_t(x_0|x_t)$ is typically modeled as a Gaussian distribution $\mathcal{N}(x_0^p; \mu(x_t, t), \sigma_t^2 I)$. Thus, the probability density function of $p_t(x_0|x_t)$ is given by:

$$p_t(x_0|x_t) = \frac{1}{\sqrt{(2\pi\sigma_t^2)^d}} \times \exp\left(-\frac{1}{2\sigma_t^2} \|x_0^p - \mu(x_t, t)\|^2\right), x_0^p \in \mathcal{T}_i. \quad (39)$$

When taking the derivative with respect to x_t , only $\mu(x_t, t)$ depends on x_t , hence:

$$\nabla_{x_t} \log p_t(x_0|x_t) = \nabla_{x_t} \left(-\frac{1}{2\sigma_t^2} \|x_0^p - \mu(x_t, t)\|^2\right) = \frac{1}{\sigma_t^2} (x_0^p - \mu(x_t, t)) \nabla_{x_t} \mu(x_t, t). \quad (40)$$

Consequently, $\nabla_{x_t} p_t(x_0|x_t)$ can be written as:

$$\begin{aligned}\nabla_{x_t} p_t(x_0|x_t) &= p_t(x_0|x_t) \frac{1}{\sigma_t^2} (x_0^p - \mu(x_t, t)) \nabla_{x_t} \mu(x_t, t) \\ &= \frac{\bar{\alpha}_t^2}{\bar{\beta}_t^2} p_t(x_0|x_t) (x_0^p - \mu(x_t, t)) \nabla_{x_t} \mu(x_t, t).\end{aligned}\quad (41)$$

We now substitute the gradient $\nabla_{x_t} p_t(x_0|x_t)$ into $\mathbb{E}_{\nabla_{x_t} p_t(x_0|x_t)} [D_{KL}(p_t(y|x_0) \| q_t(y|x_0))]$:

$$\begin{aligned}&\mathbb{E}_{\nabla_{x_t} p_t(x_0|x_t)} [D_{KL}(p_t(y|x_0) \| q_t(y|x_0))] \\ &= \int \nabla_{x_t} p_t(x_0|x_t) p_t(y|x_0) \log \frac{p_t(y|x_0)}{q_t(y|x_0)} dx_0 \\ &= \frac{\bar{\alpha}_t^2}{\bar{\beta}_t^2} \int p_t(x_0|x_t) (x_0^p - \mu(x_t, t)) \nabla_{x_t} \mu(x_t, t) p_t(y|x_0) \log \frac{p_t(y|x_0)}{q_t(y|x_0)} dx_0.\end{aligned}\quad (42)$$

Given that $p_t(x_0|x_t)$ can be expressed as $\mathcal{N}(x_0^p; \mu(x_t, t), \sigma_t^2 I)$, and $x_0^p = \frac{1}{\alpha_t} x_t^p - \frac{\bar{\beta}_t}{\alpha_t} \varepsilon$, then $\mu(x_t, t)$ can also be represented as $\frac{1}{\alpha_t} x_t^p - \frac{\bar{\beta}_t}{\alpha_t} \varepsilon_\theta(x_t^p, t)$. Consequently, the difference $x_0^p - \mu(x_t, t)$ becomes $\frac{\bar{\beta}_t}{\alpha_t} [\varepsilon_\theta(x_t^p, t) - \varepsilon]$, where $\varepsilon_\theta(x_t^p, t)$ denotes the noise prediction output of the unconditional diffusion model at time t in task \mathcal{T}_i . Similarly, the gradient $\nabla_{x_t} \mu(x_t, t)$ is given by $\frac{1}{\alpha_t} I - \frac{\bar{\beta}_t}{\alpha_t} \nabla_{x_t} \varepsilon_\theta(x_t^p, t)$, where $\nabla_{x_t} \varepsilon_\theta(x_t^p, t)$ is the Jacobian of the noise prediction model in \mathcal{T}_i . By optimizing $\varepsilon_\theta(x_t^p, t)$ to approximate ε , we implicitly optimize $\mu(x_t, t)$ and its gradient without explicitly computing $\nabla_{x_t} \mu(x_t, t)$. As a result, the term $(x_0^p - \mu(x_t, t)) \nabla_{x_t} \mu(x_t, t)$ simplifies to:

$$(x_0^p - \mu(x_t, t)) \nabla_{x_t} \mu(x_t, t) \propto \frac{\bar{\beta}_t}{\alpha_t} \|\varepsilon_\theta(x_t^p, t) - \varepsilon\|_2^2 = \frac{\bar{\beta}_t}{\alpha_t} \|\beta_t \epsilon_\theta^p + \varepsilon\|_2^2, \quad (43)$$

where this step is based on the approximations derived in Eq. 28 and Equ. 43.

Ultimately, the term for Label Knowledge Consistency can be transformed into a form that is optimizable for SDE diffusion models:

$$\begin{aligned}&\nabla_{x_t} \int \frac{p_t(x_0|x_t) p_t(y|x_0)}{p_t(y|x_t)} \log \frac{p_t(y|x_0)}{q_t(y|x_0)} dx_0 \\ &\propto \frac{\bar{\alpha}_t}{\bar{\beta}_t} \|\beta_t \epsilon_\theta^p + \varepsilon\|_2^2 \mathbb{E}_{p_t(x_0|x_t)} D_{KL}(p_t(y|x_0) \| q_t(y|x_0)), \\ &\propto \frac{\bar{\alpha}_t}{\bar{\beta}_t} \mathbb{E}_{p_t(x_0|x_t)} D_{KL}(p_t(y|x_0) \| q_t(y|x_0)),\end{aligned}\quad (44)$$

Here, the term $\|\beta_t \epsilon_\theta^p + \varepsilon\|_2^2$ involves the model parameters ϵ_θ^p optimized from the previous task and the standard normal distribution ε , making it non-optimizable. Therefore, we consider this term as a learnable scaling factor that the network can adjust on its own.

For Simplifiable Aspect term, in the context of cross-task knowledge retention via diffusion models, x_t represents the shared knowledge between tasks \mathcal{T}_i and \mathcal{T}_j . As the noise accumulates during diffusion, the correlation between x_t and the label y diminishes, reflecting the increasing abstraction of task-specific information. In this setting, the term $\nabla_{x_t} \log \frac{q_t(y|x_t)}{p_t(y|x_t)}$, which quantifies the gradient of the divergence between label-conditioned distributions across tasks, becomes increasingly insignificant. Mathematically, as x_t evolves toward a noisy state, its dependency on y weakens, and the conditional distributions of y given x_t from both tasks become approximately equal. Consequently, the gradient of their ratio $\log \frac{q_t(y|x_t)}{p_t(y|x_t)}$ tends towards zero, justifying its omission from the objective function. This simplification streamlines the optimization process, allowing the model to focus on the shared knowledge represented by x_t , while reducing the computational cost associated with task-specific label divergence and label regressor parameters, thereby improving efficiency.

As shown above, the upper bound in Equ. 33 can be expressed as:

$$\mathcal{L}_{UB} = \kappa(\epsilon_\theta^q - \epsilon_\theta^p) + \lambda \mathcal{L}_{UKC} + \eta \mathcal{L}_{LKC} = \kappa \mathcal{L}_{IKC} + \lambda \mathcal{L}_{UKC} + \eta \mathcal{L}_{LKC}, \quad (45)$$

$$\begin{cases} \mathcal{L}_{IKC} = \epsilon_{\theta}^q - \epsilon_{\theta}^p, \\ \mathcal{L}_{UKC} = \frac{\bar{\alpha}_t^2}{\beta_t^2} [\mu_{\theta}(x_t, t) - \nu_{\theta}(x_t, t)], \\ \mathcal{L}_{LKC} = \frac{\bar{\alpha}_t}{\beta_t} \mathbb{E}_{p_t(x_0|x_t)} D_{KL}(p_t(y|x_0) || q_t(y|x_0)), \end{cases} \quad (46)$$

where κ , λ , and η are weighting hyperparameters that balance the contributions of three knowledge consistency components in the total upper bound loss \mathcal{L}_{UB} .

In summary, through a detailed analysis of cross-task knowledge retention, we have developed a robust optimization strategy for shared knowledge, enabling the seamless adaptation of diffusion models across multiple tasks in continual learning scenarios. The derived loss functions, encapsulating the critical components of knowledge consistency, provide a principled approach to balancing the retention of prior task knowledge while accommodating the nuances of new tasks. This work not only furthers our understanding of diffusion models in a multi-task context but also lays the foundation for more efficient and scalable generative models capable of leveraging the inherent relationships between tasks in a dynamic, continual learning setup.

C Model Architecture Diagram

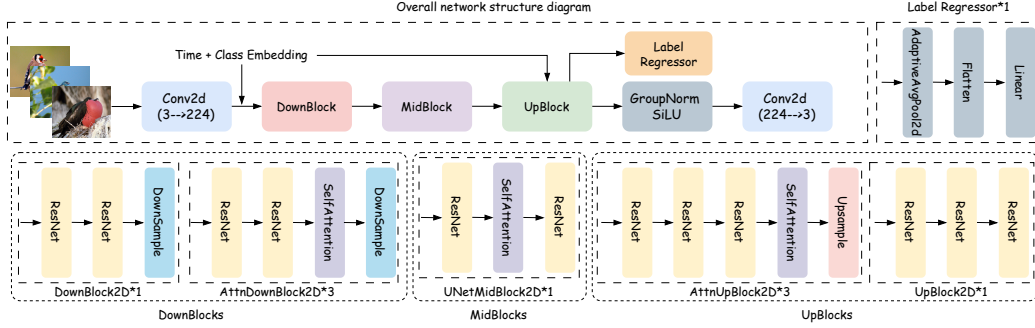


Figure 4: Overall architecture of the Continual Consistency Diffusion (CCD) model. The backbone follows a U-Net-style encoder–decoder structure with residual and attention units, and is augmented with additional heads to support intermediate knowledge consistency objectives.

Figure 4 presents a detailed schematic of the diffusion backbone used in all of our experiments. The design follows the “U-Net with cross-task hooks” blueprint popularised in contemporaneous diffusion work, but is augmented with three novel pathways that are required by the Continual Consistency Diffusion (CCD) training objective.

D Visualizations

In this section, we present the visualizations of samples generated for the first task across all datasets at the final training stage. All results are sampled based on class labels and produced using a model trained with a buffer size of 5120, ensuring a fair and unbiased comparison.

We conduct comprehensive evaluations across four continual generation benchmarks (MNIST, CIFAR100, Flowers102, and CUB200) to assess the effectiveness of our approach in retaining generative knowledge across tasks. On MNIST (Fig. 5), we observe that standard buffer-based baselines such as ER and A-GEM suffer from severe forgetting: they completely lose the ability to generate digits from the first task, including digits 0 and 1. In contrast, our method successfully reconstructs digit 0, evidencing improved knowledge retention. Nonetheless, the failure to accurately reproduce digit 1 suggests that catastrophic forgetting still persists, highlighting the need for more principled strategies for generative memory consolidation.

On the more complex CIFAR100 dataset (Fig. 6), all compared methods, including ours, fail to retain generative knowledge from the initial task. This failure can be attributed to the minimal overlap in semantic content across tasks, making cross-task knowledge retention particularly challenging.

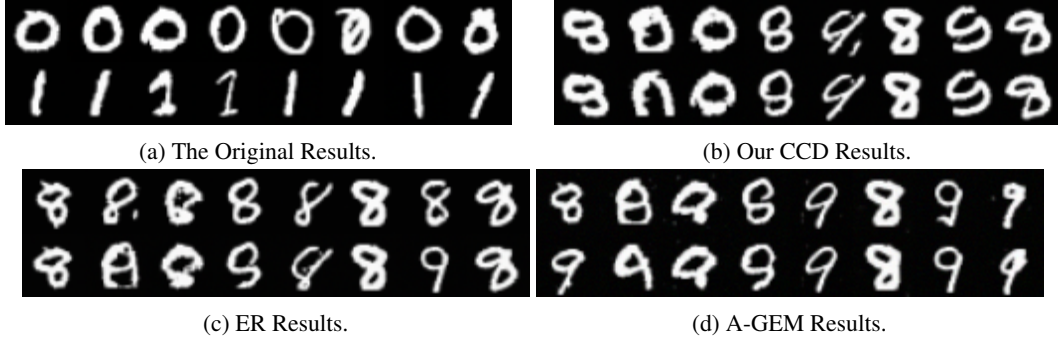


Figure 5: Comparison of generated results in 0-th task of MNIST.

These results underscore a key limitation of current approaches, including ours: the reliance on shared structural information for knowledge retention. In scenarios where such structure is absent, task interference remains severe. This raises an important open question, how can we effectively preserve and transfer independent, task-specific knowledge without impeding the acquisition of new information?

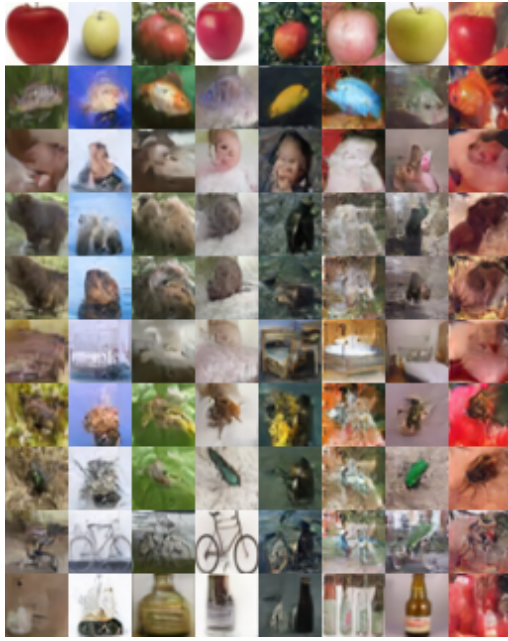
In the Flowers102 benchmark (Fig. 7), where the dataset size is comparable to the buffer capacity, all methods achieve moderate generative performance. However, qualitative differences are evident. Our model consistently generates samples with higher visual fidelity and stronger alignment to real data. For instance, it successfully captures rare instances, such as white flowers in the third category, that A-GEM entirely fails to reproduce. Moreover, in categories prone to error (e.g., the seventh category), our model avoids semantic drift and maintains accurate class representation, suggesting a stronger capacity for handling underrepresented classes.

Finally, on CUB200, a fine-grained benchmark (Fig. 8), our method clearly outperforms baselines in generative memory retention. It successfully reconstructs samples from the initial task, while ER and A-GEM fail to recover any meaningful representations. The alignment between fine-grained structure and our design principle of knowledge propagation yields consistently better generative fidelity. These findings not only validate our theoretical formulation but also demonstrate the practical advantage of our method in continual generation settings that demand nuanced representation learning.

In summary, our approach shows strong resilience to forgetting, particularly in tasks with shared visual structure or fine-grained semantics. However, the limitations observed in unstructured task regimes, such as CIFAR100, emphasize the need for future work to address the preservation of task-specific knowledge in the absence of inter-task alignment.

E Future Improvements

(1) *Hyper-parameter Sensitivity*: The method depends on three hyper-parameters, whose optimal values vary across datasets. For instance, while MNIST settings may be effective, other datasets perform best with all values around $1e-7$. Future work should explore adaptive tuning strategies to improve robustness across datasets. (2) *Buffer Quality*: The metrics on CIFAR100-10T reveals that a larger buffer size (2560 or 5120) underperforms compared to a smaller buffer (512), suggesting that for certain datasets, the quality of stored samples is more critical than quantity.



(a) The Original Results.



(b) Our CCD Results.



(c) ER Results.

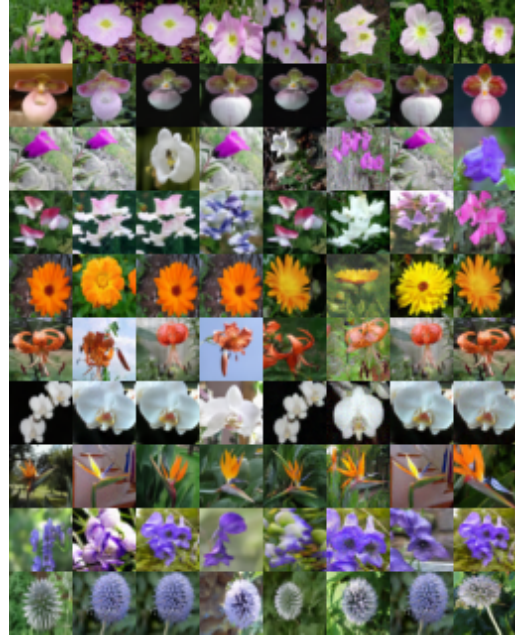


(d) A-GEM Results.

Figure 6: Comparison of generated results in the 0-th task of CIFAR100.



(a) The Original Results.



(b) Our CCD Results.



(c) ER Results.



(d) A-GEM Results.

Figure 7: Comparison of generated results in the 0-th task of Flowers102.

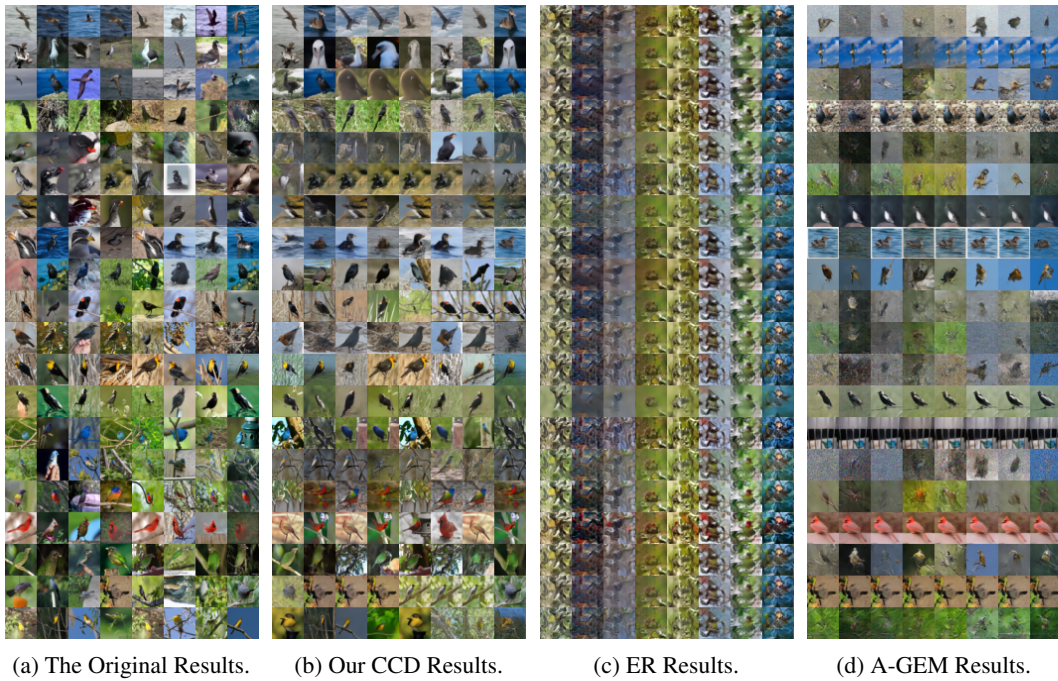


Figure 8: Comparison of generated results in the 0-th task of CUB200.